Journal of Sound and Vibration (1998) **211**(4), 663–681

A BEM APPROACH TO ASSESS THE ACOUSTIC PERFORMANCE OF NOISE BARRIERS IN A REFRACTING ATMOSPHERE

K. M. Li and Q. Wang

Engineering Mechanics Discipline, *Faculty of Technology*, *The Open University*, *Walton Hall*, *Milton Keynes MK7 6AA*, *England*

(*Received* 30 *July* 1997, *and in final form* 25 *November* 1997)

Theoretical and experimental investigations into the acoustic performance of noise barriers in a refracting atmosphere are presented. The theory is based on the conformal transformation. It can be shown that the sound field in a refracting atmosphere with an exponential sound speed profile above a flat impedance ground is identical to the sound field in the homogeneous medium above a cylindrically curved impedance surface. The sound fields behind noise barriers can then be computed accurately by means of the Boundary Element Method (BEM). In addition, a scale model study has been conducted for experimental investigations of the sound diffraction behind thin barriers above cylindrically curved surfaces. These experimental results validate the proposed numerical scheme. Finally, the BEM is extended to predict the sound fields, in both the upward and downward refracting atmosphere, behind a thin barrier up to a range of 110 m. Also the numerical predictions based on the BEM are compared with other published experimental results.

1. INTRODUCTION

In the past 30 years, noise control by barriers has become increasingly common as an effective measure for environmental protection against transportation and other noise sources by blocking the "line-of-sight" between source and receiver. The noise levels are significantly reduced because only a small proportion of sound energy is received by the "listener" via diffraction over the top of (or the end of) a barrier. The introduction of and reports on the use of barriers for the control of traffic noise can be dated back to the 1960s in the U.K. [1–3], and in other countries (see, for example, references [4–7]). More recently, the installation of noise barriers on the M25 between junctions 10 and 11 has been reported by Johnston [8]. To date, much effort has been devoted to predict the sound levels behind barriers by means of theoretical studies, scale-model experiments and other more costly full scale field measurements [9]. In the past, rules and charts have been devised which combine theoretical approximations and field experience heuristically [4]. These rules or charts aid the practical design of noise barriers. Much of this early theoretical work is based on classical diffraction theory (see, for example, references [10, 11]). More recent theoretical work allows the presence of an impedance ground, the use of sound-absorbent materials on the barrier surface [12, 13], and finite length barriers [14, 15]. Also a computationally intensive scheme known as the boundary element method (BEM) has been used widely [16] in recent years due to the advent of digital computers.

Despite extensive literature and research in this area, it is commonly found that the insertion loss of barriers measured outdoors is often much lower than predicted by theory

0022–460X/98/140663 + 19 $25.00/0/sv971427

or measured with models in anechoic chambers [1, 7]. The discrepancies are in part due to the influence of meteorological conditions, as in most previous theoretical studies the effects of turbulence, wind and temperature gradients were ignored. In this context, there is a need to redress the balance by investigating the meteorological influence on the performance of noise barriers. Hence the work reported here is a study of the degradation of a barrier's performance under the influence of adverse meteorological conditions. The effects of atmospheric turbulence are ignored in the current study. This information is particularly useful in drafting guidelines for the design of noise barriers.

The propagation of sound over an impedance ground containing a barrier and in an inhomogeneous atmosphere is an important topic of study. In predicting such propagation, two numerical approaches have been suggested in the literature. If the atmosphere is homogeneous, the boundary element method (BEM) is more suitable than the parabolic equation (PE) method for tackling the problem. The BEM approach takes back-scattering into account while the PE method ignores the back-scattered field. If the atmosphere is inhomogeneous then the PE method is superior but only as long as there is no significant back-scatter. Typical examples of such situations are the case of the sound field in front of a tall barrier, steep hills or tree belts. Real atmospheric environments will be inhomogeneous and may involve insignificant back-scatter. Nevertheless, Salomons [17] has used the PE method and a semi-empirical ray-based scheme to predict the sound field behind noise barriers in the refracting atmosphere. However, in this paper, the BEM scheme is used to predict the meteorological influence on the acoustic performance of noise barriers. Numerical results are validated by laboratory experiments and the scheme is used to predict the sound field behind a thin barrier in a refracting atmosphere.

2. THEORETICAL FORMULATION AND ITS VALIDATION

The model considered is that of a sound field due to a point source above a ground surface with or without a barrier. The atmosphere is assumed to be vertically stratified such that the effective sound speed profile depends only on the vertical height, z, above the ground. The effect of atmospheric turbulence has been ignored in the present study. Suppose that the source is located at $(0, 0, h_s)$ and the barrier is a two-dimensional one with uniform cross-section along its length which is parallel to the y-axis as shown in Figure 1. Furthermore, the barrier may be considered as a hard screen with a negligible thickness, maximum height of h_b, and located at a distance x_b from the source. The analysis is restricted to a two-dimensional situation with a flat ground at $z = 0$. Without loss of

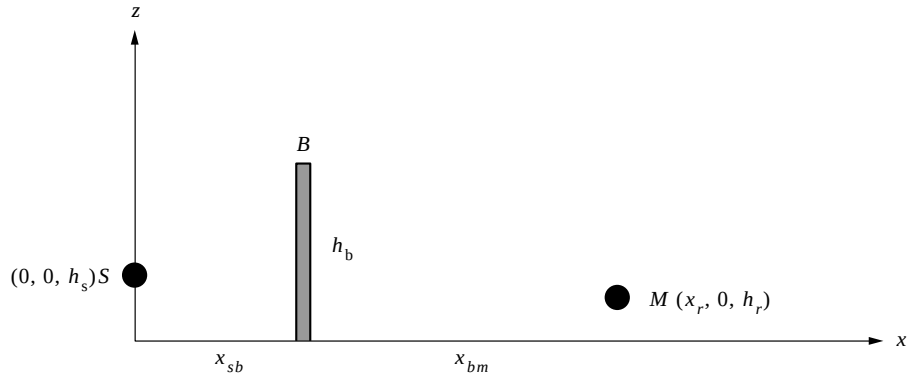

Figure 1. Sketch illustrating a two-dimensional barrier with uniform cross-section along its length parallel to the y-axis inserting between a source and receiver.

generality, it is assumed that the source and receiver are situated on the plane $y = 0$. The source and receiver are separated by the barrier with the receiver located at $(x_r, 0, h_r)$ with $x_r > x_b$. The sound field at the receiver can be determined by solving the two-dimensional Helmholtz equation

$$\partial^2 p/\partial x^2 + \partial^2 p/\partial z^2 + k^2(z)p = -\delta(x)\delta(z - h_s), \tag{1}$$

where $p(x, z)$ is the acoustic pressure, $k(z) \equiv 2\pi f/c(z)$, is the wavenumber, f is the source frequency, $c(z)$ is the effective sound speed and the time dependent factor $\exp(-i\omega t)$ is understood. In addition to the governing Helmholtz equation, the acoustic pressure is also subjected to the following boundary conditions: (1) the impedance boundary condition, at $z = 0$,

$$\partial p/\partial z + ik_0\,\beta(x)p = 0; \tag{2a}$$

(2) the barrier boundary condition, at $x = x_b$ and $0 \leqslant z \leqslant h_b$,

$$\partial p/\partial x + ik_0\,\beta_b\,p = 0; \tag{2b}$$

(3) the Sommerfeld radiation condition as $r \to \infty$, where $r = \sqrt{x^2 + z^2}$,

$$\sqrt{r}\,(\partial p/\partial r - ik_0\,p) = 0. \tag{2c}$$

Here, in equations (2a)–(c), $k_0 \equiv k(0)$ is the reference wavenumber, β_b is the specific normalized admittance of the barrier (which is zero for a hard barrier), and $\beta(x)$ is the specific normalized admittance of the ground which may vary as a function of x at the plane of $z = 0$.

A rigorous numerical approach is to be used to compute the sound fields by means of the boundary element method (BEM). The approach is based on the application of the boundary integral equation method to the governing Helmholtz equation [18]. A major drawback of the application of the BEM is that it requires the general solution, or the so-called Green function, for equation (1) in the absence of barriers. A closed form analytic solution for an arbitrary sound speed gradient is difficult to derive. To date, closed form analytic solutions exist only for a homogeneous medium and for a limited class of well defined sound speed profiles. An example of such well-known solutions is that of a linear sound speed profile. Li *et al*. [19] have developed the BEM to compute the scattering of sound due to a Gaussian bump or trough for such a sound speed profile. However, their analytic Green function involves modified Bessel functions and Legendre functions of the second kind that are rather complicated and difficult to compute accurately. Thus, it is desirable to use the existing BEM program code [18] (that is only suitable for a homogeneous medium) to assess the effect of the refracting atmosphere on the performance of noise barriers. To this end, one can use a conformal transformation that allows one to transform equation (1) to a simplified form: i.e., for a medium with a constant wavenumber k at the expense of "distorting" the boundary surfaces. This may lead to a somewhat more complicated boundary condition. Since numerical solutions are sought, the added complication in the boundary condition will not, in principle, pose any numerical difficulty in computing the sound field.

In a recent study, Li *et al*. [20] have rigorously investigated the acoustic analogy for the sound field above a cylindrical convex curve surface in a homogeneous atmosphere and that above a flat ground in an upward refracting atmosphere. One assumes an exponential sound speed profile in which the wavenumber, $k(z)$, in equation (1) can be expressed as

$$k(z) = k_0 \exp(z/R_c), \tag{3}$$

where R_c is the radius of curvature of launched rays. This form is particularly useful because it approximates a linearly decreasing sound speed for small z/R_c,

$$c(z) \approx c(0)\,(1 - z/R_c),$$

where $c(z)$ is the speed of sound. By means of a conformal transformation [21] one can set

$$X = R_c \exp(z/R_c)\cos(x/R_c + \varphi_s), \qquad Z = R_c \exp(z/R_c)\sin(x/R_c + \varphi_s), \tag{4}$$

where φ_s is an arbitrary constant angle specified in Figure 2. Upon introducing a Jacobian factor, $J[\equiv |\partial(X, Z)/\partial(x, z)|]$, it is straightforward to show the following identities:

$$J = \left|\frac{\partial(X, Z)}{\partial(x, z)}\right| = \exp(2z/R_c), \qquad \frac{\partial^2 p}{\partial x^2} + \frac{\partial^2 p}{\partial z^2} = J \times \left(\frac{\partial^2 p}{\partial X^2} + \frac{\partial^2 p}{\partial Z^2}\right), \tag{5a, b}$$

and

$$\delta(x - x_s)\delta(z - z_s) = J\delta(X - X_s)\delta(Z - Z_s), \tag{5c}$$

where the source position, (X_s, Z_s) is determined according to equation (4) (with $x = x_s = 0$ and $z = h_s$) to give $R_c \exp(h_s/R_c)\cos\varphi_s$ and $R_c \exp(h_s/R_c)\sin\varphi_s$, respectively. Substitution of equations (5b) and (5c) into equation (1) leads to

$$\partial^2 p/\partial X^2 + \partial^2 p/\partial Z^2 + k_0^2 p = -\delta(X - X_s)\delta(Z - Z_s), \tag{6}$$

because J is factored out as it is present in every term. The corresponding boundary conditions, see equations (2a)–(2c), are transformed to the following: (1) the impedance boundary condition, at $R = R_c$,

$$\partial p/\partial R + \mathrm{i}k_0 \beta p = 0; \tag{7a}$$

(2) the barrier boundary condition, at $\Theta = \Theta_b$ and $R_c \leqslant R \leqslant R_b$,

$$\partial p/\partial x + \mathrm{i}k_0 \beta_b(\Theta) p = 0; \tag{7b}$$

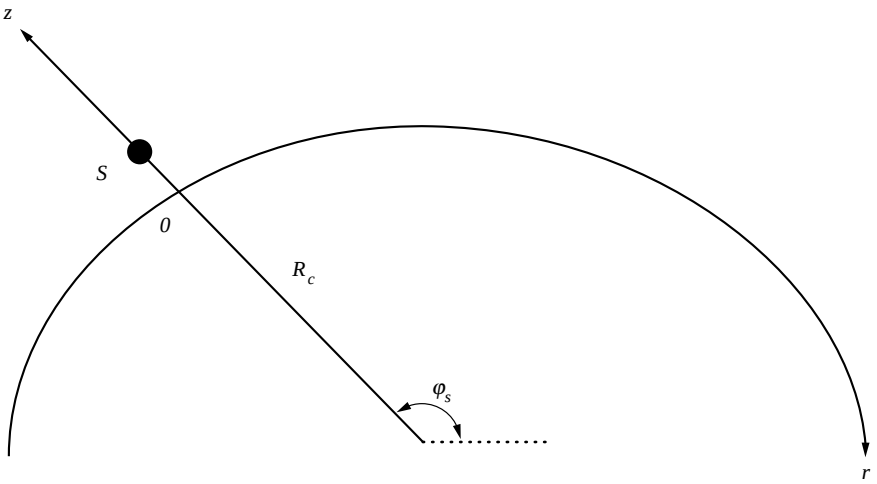

Figure 2. Illustration of a conformal transformation system.

(3) the Sommerfeld radiation condition, as $R \to \infty$,

$$\sqrt{R}\,(\partial p/\partial R - \mathrm{i}k_0\, p) = 0, \tag{7c}$$

where (R, Θ) is the polar co-ordinate of the field point in the transformed space: i.e.,

$$R = \sqrt{X^2 + Z^2} = R_c \exp(z/R_c), \qquad \Theta = \tan^{-1}(Z/X) = (x/R_c) + \varphi_s. \tag{8a, b}$$

The quantity $R_b \equiv R_c \exp(h_b/R_c)$ is the corresponding radius of the maximum height of the barrier.

In typical outdoor conditions, R_c is of the order of 1 km. It is reasonable to assume

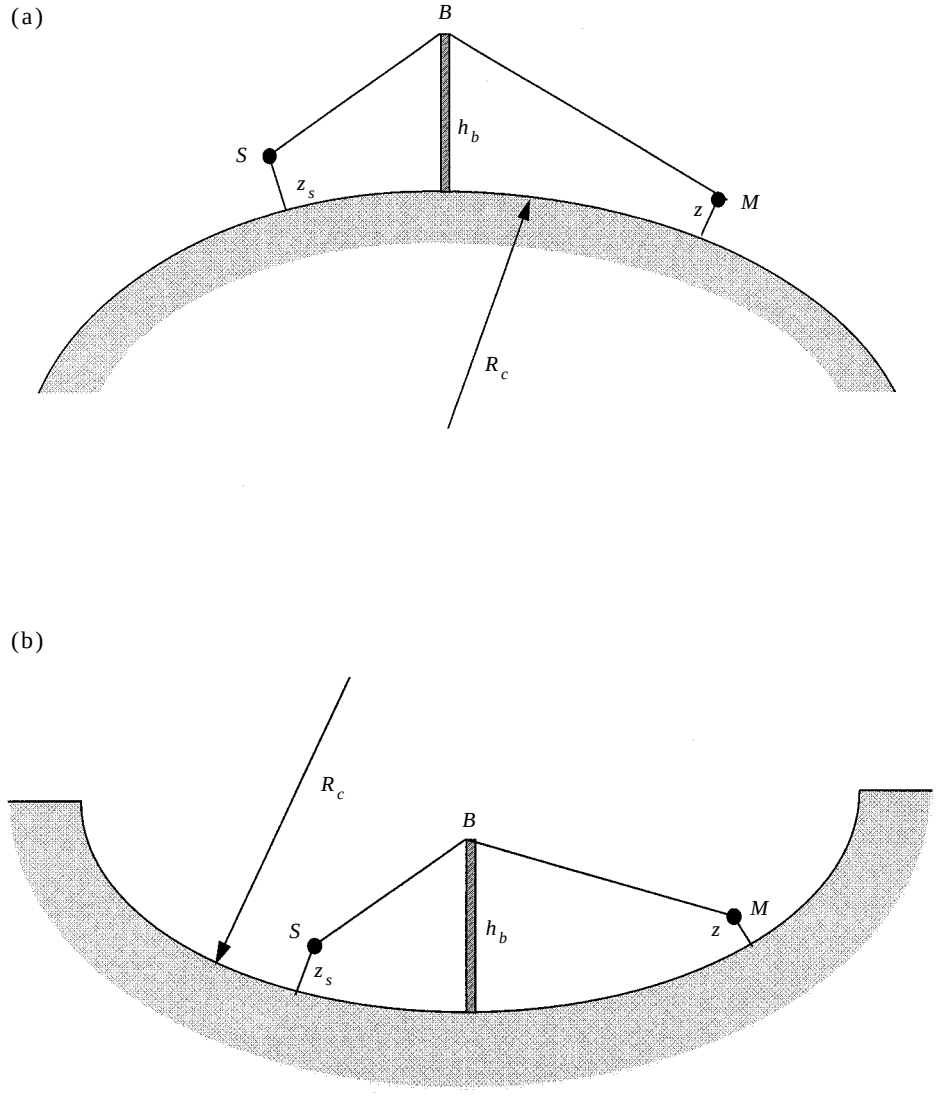

Figure 3. Sketch illustrating the analogy between: (a) upwardly curved ray path above a flat boundary and straight line propagation above a convex surface; (b) downwardly curved ray path above a flat boundary and straight line propagation above a concave surface, in the presence of a barrier (reflected waves not shown).

$R_c \gg \max(h_s, h_r, h_b)$. Furthermore, attention can be restricted to a relative short range, X_r such that R_c is greater X_r. Then one obtains the approximations

$$R \approx R_c + z \qquad \text{and} \qquad R_b \approx R_c + h_b. \tag{9}$$

Therefore the posed problem is equivalent to the calculation of the sound field due to a point source of unit strength in a homogeneous medium. The source is placed above a large convex circular cylinder and the barrier is located along a radial length of a constant polar angle. See Figure 3(a) for the configuration.

Similarly, the corresponding acoustic analogy exists for the sound field above a cylindrical concave curve surface in a homogeneous atmosphere and that above a flat ground in a downward refracting atmosphere. One can use the analogous analysis as above with the effective sound speed given by

$$c(z) = c(0)\exp(z/R_c), \tag{10}$$

that approximates a linearly increasing sound speed gradient of $c(0)[1 + Z/R_c]$. It is straightforward to show the problem posed is equivalent to the computation of the sound field due to a point source in a homogeneous medium above a cylindrical concave curve surface, see Figure 3(b). The BEM has proved to be an efficient and accurate numerical tool for solving the class of problem described above: i.e., the sound field above a curved boundary surface in a homogeneous medium. Its numerical procedure is fairly standard and the details have been described elsewhere [18].

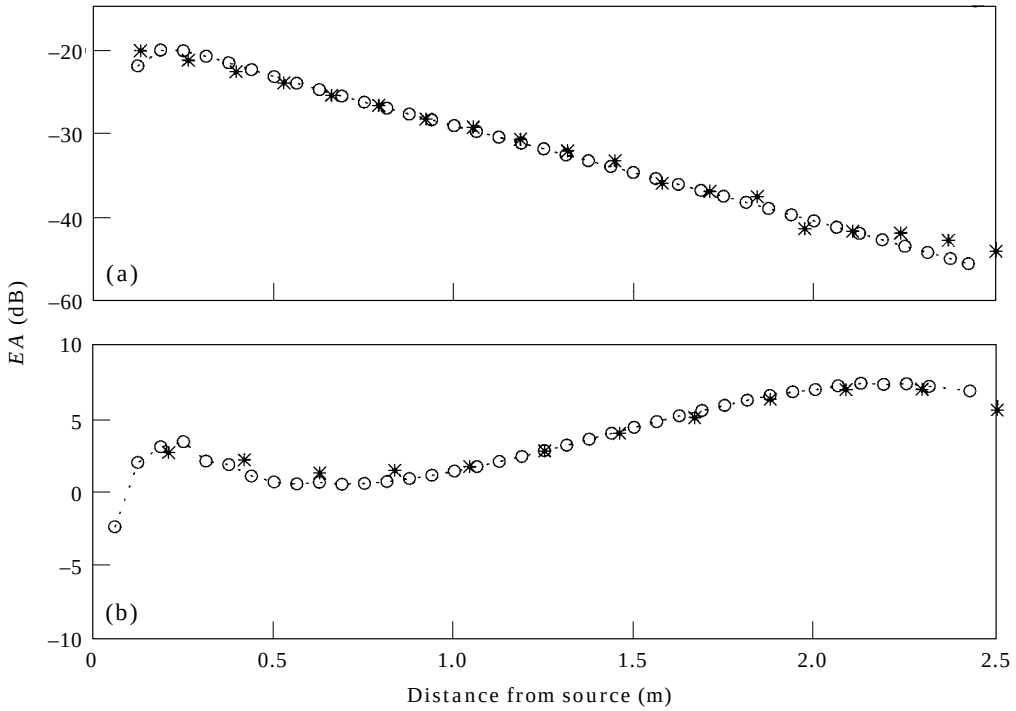

Figure 4. Excess attenuation calculated by the BEM and CERL-FFP with $R_c = 2{\cdot}5$ m, $\sigma_e = 38$ kPa s^{-1} m^{-2}, $\alpha_e = 15$ m^{-1}, $h_s = 0{\cdot}1$ m and $h_b = 0$. (a) Upward refracting medium, for a frequency of 4 kHz and $h_r = 0{\cdot}0$ m; (b) downward refracting medium, for a frequency of 2·9 kHz and $h_r = 1{\cdot}2$ m. Circles and dotted lines: BEM calculations; stars: CERL-FFP calculations.

To validate the use of BEM in the refracting atmosphere, one can first compare the numerical results according to the BEM and the fast field program (FFP) [22]. In these calculations, it is assumed that there is no barrier between the source and receiver: i.e., $h_b = 0$. Figures 4(a) and (b) are, respectively, the plots for the prediction of the sound field in an upward and a downward refracting atmosphere. A two-parameter variable porosity model [23] for ground admittance, β, is used throughout the paper, with

$$\beta = \frac{1}{0{\cdot}436(1 + \mathrm{i})\sqrt{\sigma_e / f} + 19{\cdot}48\alpha_e / f}, \tag{11}$$

where σ_e and α_e are the effective flow resistivity and effective rate of change of porosity with depth. The radius of curvature of the curve surface, R_c is chosen to be 2·5 m and two

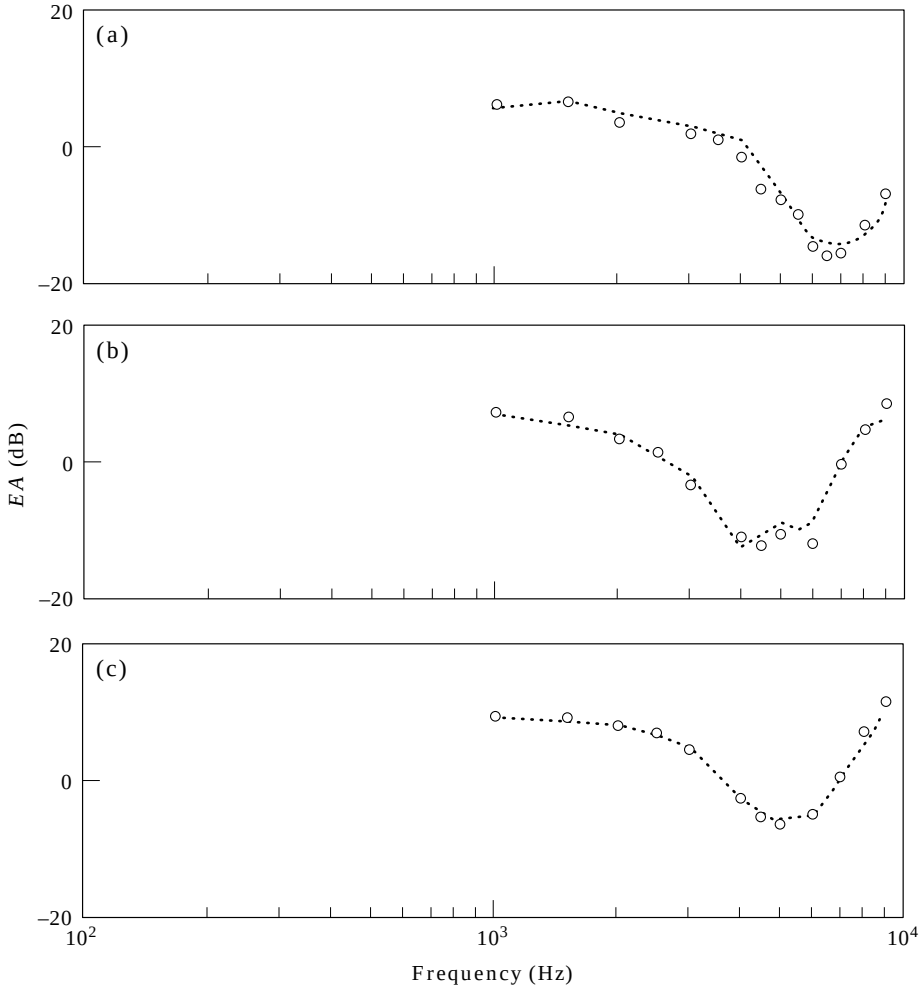

Figure 5. Excess attenuation versus frequency obtained behind a barrier on a rigid concave surface with $R_c = 20$ m, $h_b = 0{\cdot}8$ m, $x_{sb} = 4$ m and $h_s = 0{\cdot}1$ m. (a) $h_r = 0{\cdot}05$ m, $x_r = 5$ m; (b) $h_r = 0{\cdot}15$ m, $x_r = 6$ m; and (c) $h_r = 0{\cdot}1$ m, $x_r = 7$ m. Circles: BEM calculations; dotted lines: measurements [26].

frequencies, 4 and 2·9 kHz, are used in the calculations. In addition, the ground impedance surface is chosen with $\sigma_e = 38$ kPa s^{-1} m^{-2} and $\alpha_e = 15$ m^{-1}. Note that similar parameter values for the ground impedance have also been found in an outdoor measurement of grassland at an airfield [24]. The fast field program is based on the computation of an inverse Hankel transform [22] for the exponential sound speed profile. A strong gradient with R_c of 20 m and a relatively soft ground are used in these calculations. The choice of these parameters reflects the radius and the impedance of the curve surfaces used in subsequent laboratory measurements. A weaker gradient means a larger radius of curvature and hence more "elements" are required in the BEM computations. Figure 4(a), shows comparisons for the upward refracting atmosphere with the source frequency of 4 kHz, and the source and receiver heights at 0·1 and 0·0 m, respectively. Figure 4(b) displays the numerical results for the downward refracting atmosphere with the source frequency of 2·9 kHz, and the source and receiver heights at 0·1 and 1·2 m, respectively. Generally speaking, the agreements between the numerical solutions due to the BEM and the FFP solutions are excellent for both the upward and the downward refracting medium. The agreements are less satisfactory for a high source or receiver height and for a longer range (these numerical comparisons will not be shown here) because of the inherent approximations; see equation (9).

Next, numerical results are presented as calculated by the BEM for a barrier on a rigid concave surface. These numerical results are used to compare with an earlier experimental and theoretical studies by Gabillet *et al*. [25] in which a Gaussian beam approach is used

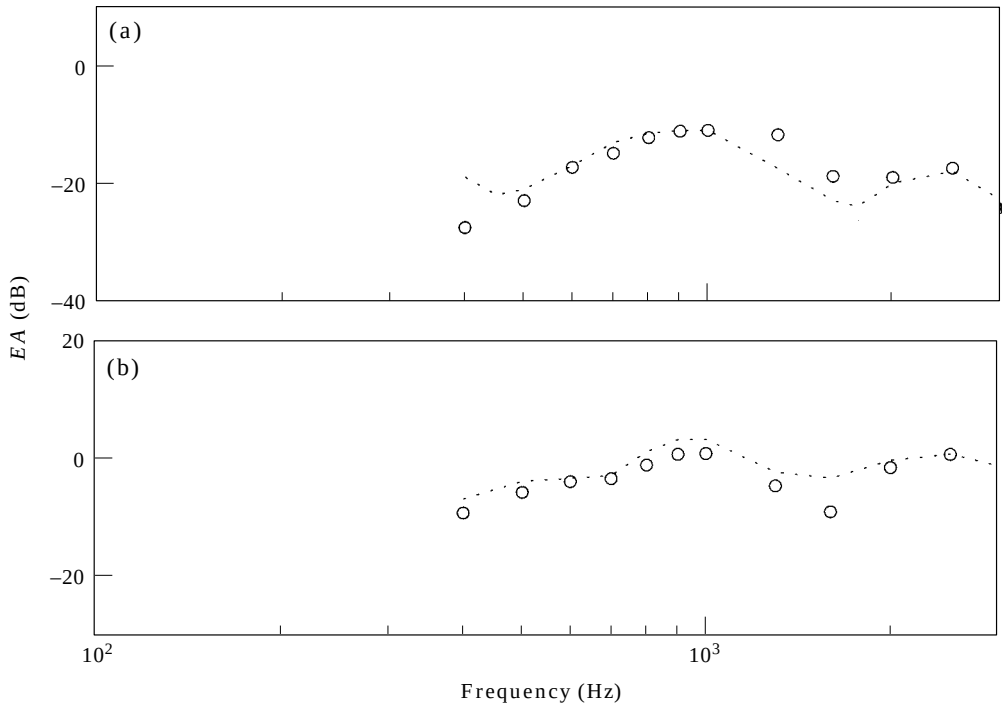

Figure 6. Excess attenuation obtained above an absorbing ground with $\sigma_e = 20$ kPa s^{-1} m^{-2}, $\alpha_e = 60$ m^{-1} and gradients of $\mp 2{\cdot}9 \times 10^{-3}$ m^{-1}. $h_s = 2$ m, $h_r = 1$ m, $h_b = 2{\cdot}5$ m. Dotted lines: Rasmussen's measurements; circles: the BEM calculations. (a) Upwind, $x_{sb} = 40$ m and $x_{bm} = 20$ m; (b) downwind, $x_{sb} = 20$ m and $x_{bm} = 40$ m.

to predict the sound field in a downward refracting atmosphere. In their experimental measurements, Gabillet *et al*. used a barrier height of 0·15 m, a curved surface radius, R_c of 20 m and a source height of 0·1 m. Figure 5 shows the BEM calculations (circles) and their measured spectra (dotted lines) that are taken directly from Figure 15 of reference [25]. The numerical results are presented in terms of excess attenuation, equivalent to their relative sound pressure levels. Figure 5(a) shows the results for the range of 5 m and receiver height of 0·05 m. Here, in this example, the receiver is located deep in the shadow zone of the barrier. Figure 5(b) shows the results for the range of 6 m and receiver height of 0·15 m. The receiver is located in close proximity to the limiting ray of the shadow boundary in this case. Finally, Figure 5(c) displays results obtained for the receiver further away from the barrier with the range of 7 m and receiver height of 0·1 m. In all cases, there are excellent agreements between the BEM predictions and the Gabillet *et al*. experimental measurements. Their Gaussian beam predictions are not shown in Figures 5(a)–(c) for the clarity of presentation.

Numerical results calculated by the BEM for a barrier in the refracting atmosphere are also presented, to compare them with Rasmussen's scale model measurements conducted in a wind tunnel for upwind and downwind conditions [26]. In his experimental analyses, Rasmussen represented the wind velocity gradients by a set of linear profiles. Figures 6(a) and 6(b) show his experimental results and the predictions based on the BEM approach. In our numerical analyses, the BEM with a constant effective sound velocity gradient of $2{\cdot}9 \times 10^{-3}\,\mathrm{m}^{-1}$ was used. The other parameters, such as source height, receiver height, range (they are respectively, 2, 1 and 60 m) and the ground impedance (two-parameter variable porosity model with $\sigma_e = 20\,\mathrm{kPa\,s^{-1}\,m^{-2}}$ and $\alpha_e = 60\,\mathrm{m^{-1}}$), are identical to those used by Rasmussen. In these figures, the dotted curves are taken directly from Figures 9 and 10 of reference [26], while the circles are the BEM calculations. The numerical result are presented in terms of excess attenuation, equivalent to the sound-pressure level *re* free field used in reference [26]. In spite of the use of the approximate constant sound speed gradient, the agreement is very good in both upwind and downwind situations between the present BEM predictions and Rasmussen's measured frequency spectra.

From these comparisons with other results, it is obvious that the BEM is a valid and accurate numerical tool to study the acoustic performance of noise barriers in the presence of temperature gradients. Furthermore, it is enlightening to confirm that a cylindrical curved surface may be used as a convenient alternative to the use of a wind tunnel [26, 27] in the current study. The following section is devoted to experimental investigations of the sound field in the refracting atmosphere behind a barrier.

3. SCALE MODEL EXPERIMENTS

A series of model experiments was conducted with a scale of 1 : 8. To simulate the refracting atmosphere in an indoor environment, two types of cylindrical curved (a concave and a convex) surfaces were required in the experiments. Both surfaces were constructed by overlying sheets of masonite attached to corresponding wooden frames. Both frames consist of a long cylinder with a constant cross-sectional area and have a radius of curvature of 2·5 m. The convex curved surface corresponds to the external surface of a cylinder while the concave curved surface corresponds to the internal surface of a cylinder. They were built to have a centerline of 2·5 m, a span of 1·8 m and a height of 0·45 m. A carpet felt with a thickness of 16 mm was laid on top of the wooden frames in order to simulate an impedance ground. The carpet felt was secured to the wooden frame by using double sided tapes to eliminate the possible transmission path between the wooden surface and the felt. In an early acoustical characterization of the carpet felt, it was found that

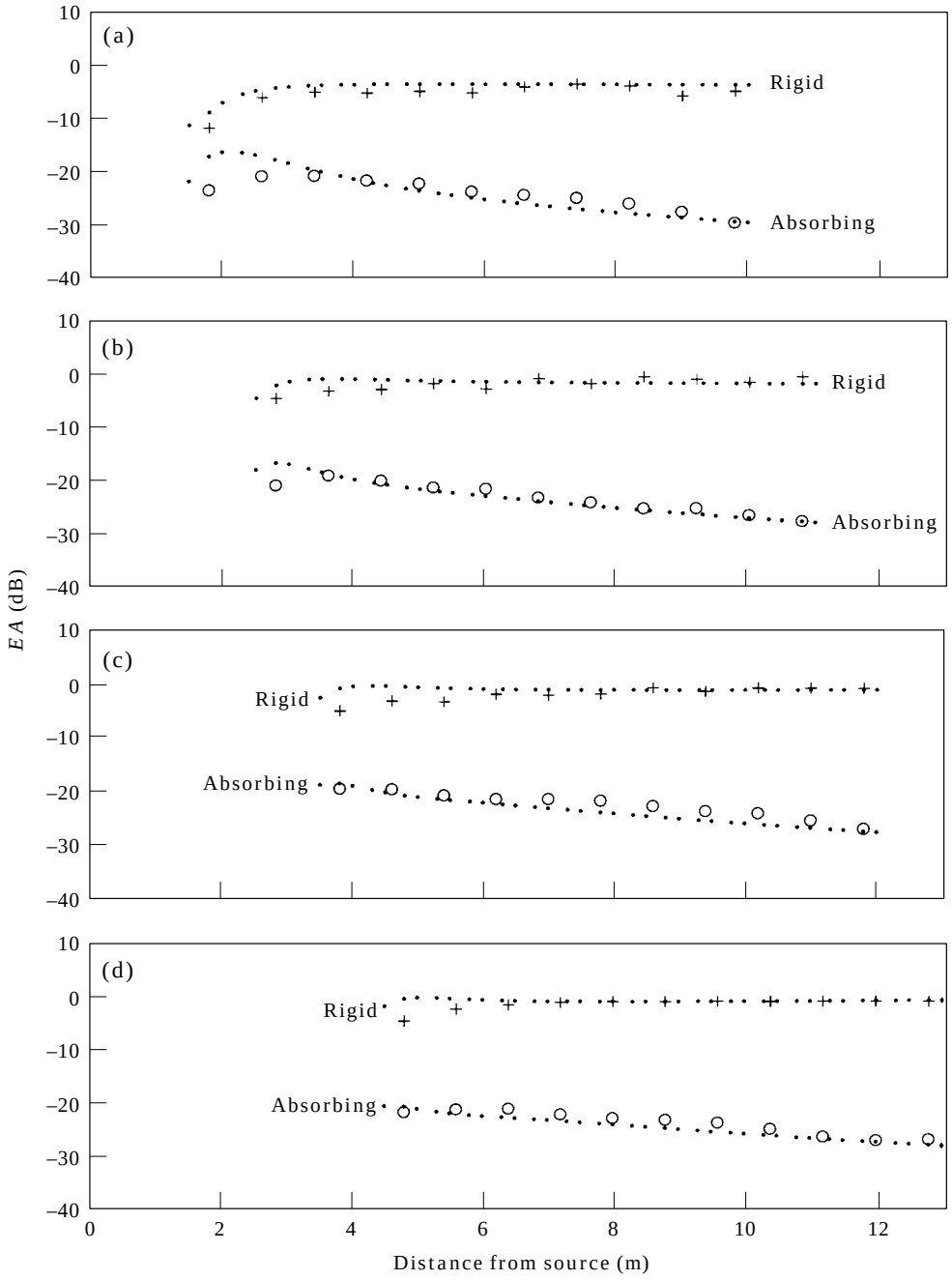

Figure 7. Excess attenuation obtained for a frequency of 500 Hz over flat surfaces in the presence of a barrier. Points: the boundary element method calculations; circles and cross: experimental measurements. $h_s = 0{\cdot}16$ m, $h_r = 0{\cdot}05$ m, $h_b = 0{\cdot}80$ m, x_{sb} = (a) 1·0 m, (b) 2·0 m, (c) 3·0 m, and (d) 4·0 m.

the two-parameter variable porosity model with $\sigma_e = 38$ kPa s m^{-2} and $\alpha_e = 15$ m^{-1} allowed best agreements between the theoretical predictions and experimental characterizations [28]. These parameters are substituted into equation (11) in order to determine the specific normalized admittance of the ground surface. To compare with the barrier attenuation in the homogeneous atmosphere, measurements were conducted also over a rigid flat board and a felt-covered flat board.

The curved surfaces and the flat board were placed, in turn, in an anechoic chamber of dimension $3 \times 3 \times 3$ m. A quarter-inch condenser microphone fitted with pre-amplifier was used to measure the sound pressure levels. A Tannoy speaker fitted with a 3-cm internal diameter long tube of 90 cm was used as a point monopole source. A PC-based system analyser, Maximum Length Sequence System Analyzer (MLSSA), was used both as the generator for the speakers and as the analyser for subsequent signal processing.

A long thin edge stainless steel sheet of thickness 3 mm and height of 0·1 m was used to simulate a thin barrier that is placed on the top of the convex or concave surfaces. The barrier was perpendicular to the centerline of the curved surfaces. The bottom edge of the barrier was sealed by using Bostik blu-tack™ in order to avoid the possible "leakage" of sound through the gap between the barrier and curved surfaces.

As the diffraction of sound depends strongly upon the source/receiver geometry, the source and receiver heights were kept constant in all measurements with scaled heights of $h_s = 0{\cdot}16$ m and $h_r = 0{\cdot}005$ m (the actual source and receiver heights were 20 and 6·4 mm, respectively). Initial measurements were conducted in the absence of the barrier over the flat board, and the curved surfaces. Different measurements were then made with the barrier inserted at scaled distances of 1, 2, 3 and 4 m from the source. The height of the scaled barrier was 0·8 m (the actual barrier height was 0·1 m). A scaled frequency of 500 Hz was used (the actual frequency of the noise source was 4 kHz) in the measurements. The parameters for the source/receiver geometry and frequencies were adjusted to reflect the fact that scale model experiments were conducted.

A scale factor of 1 : 8 was used in the study but there was no corresponding scaling for the impedance of the ground surface. The specific normalized admittance of the ground was determined to be 0·3524–0·3715i for 500 Hz. The use of a scale model enables an efficient and accurate use of the BEM to be made in the computation of the sound fields behind the barrier. Note that a scaled frequency of 375 Hz (actual frequency of 3 kHz) has also been used in the measurements. Nevertheless, the experimental results show a rather similar trend. Consequently, these experimental results are not reported here for brevity. Details of these measurements can be found elsewhere [28].

4. EXPERIMENTAL RESULTS AND COMPARISON WITH BEM PREDICTIONS

Hothersall *et al*. [16] have conducted extensive measurements to validate the BEM for a similar problem of a barrier over a flat ground. In the present situation, a flat board was used as our first test case in order to confirm the validity of the scale model used in the experimental investigations. In the following plots, excess attenuation (EA) is defined as the sound field above an impedance ground relative to the sound field in the absence of any boundary plane. Figure 7 shows the measurements and BEM predictions above flat rigid and absorbing ground surfaces and with the barrier situated at various distances from the source. Figure 7 shows typical results above the flat surface for a source frequency of 500 Hz in these particular examples. In general, the agreement between the experimental measurements and the BEM predictions is excellent. This, in turn, validates use of the scale model in the measurements.

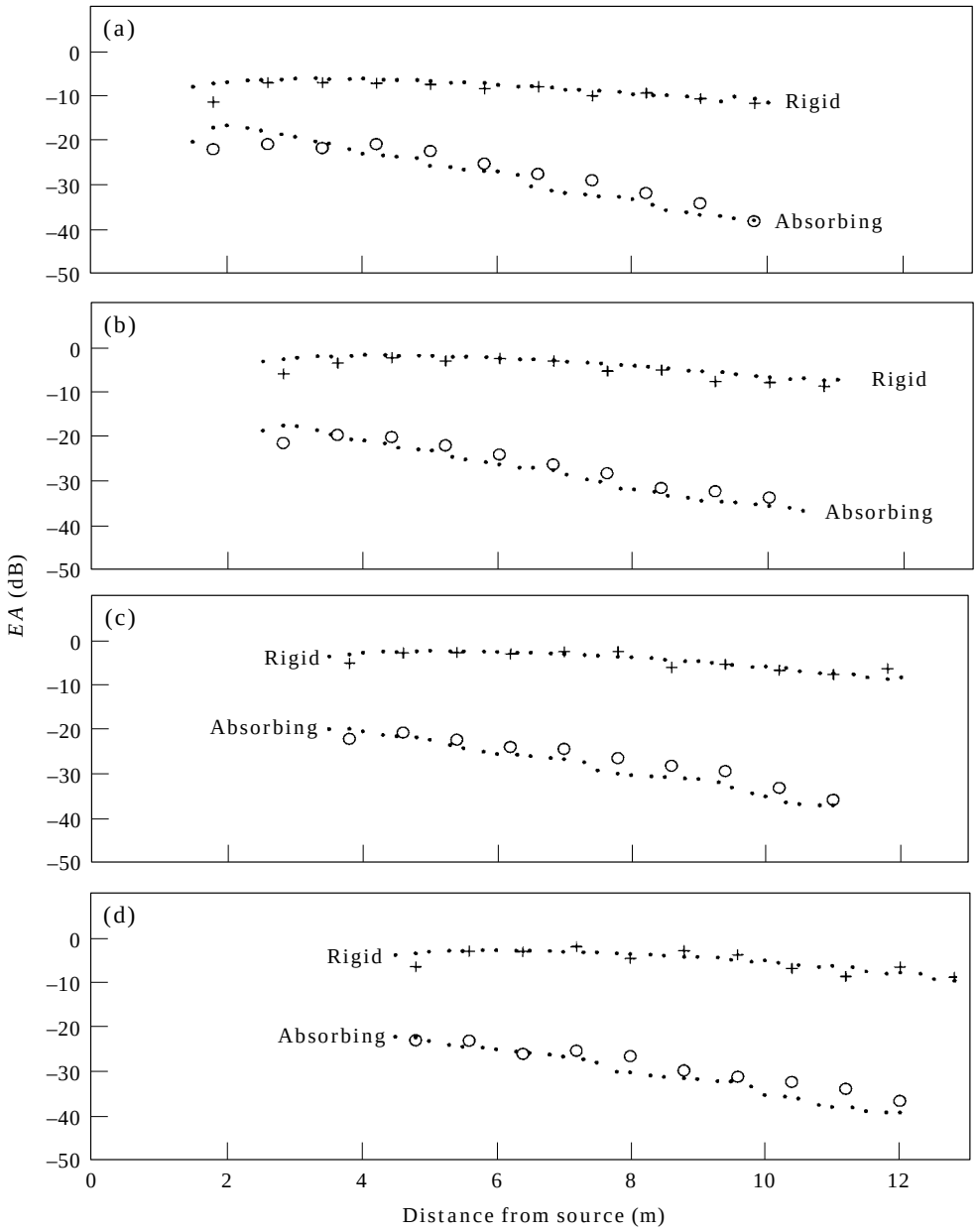

Figure 8. Excess attenuation obtained for a frequency of 500 Hz over convex surfaces in the presence of a barrier. Points: the boundary element method calculations; circles and pulses: experimental measurements. $h_s = 0{\cdot}16$ m, $h_r = 0{\cdot}05$ m, $h_b = 0{\cdot}80$ m, x_{sb} = (a) 1·0 m, (b) 2·0 m, (c) 3·0 m, and (d) 4·0 m.

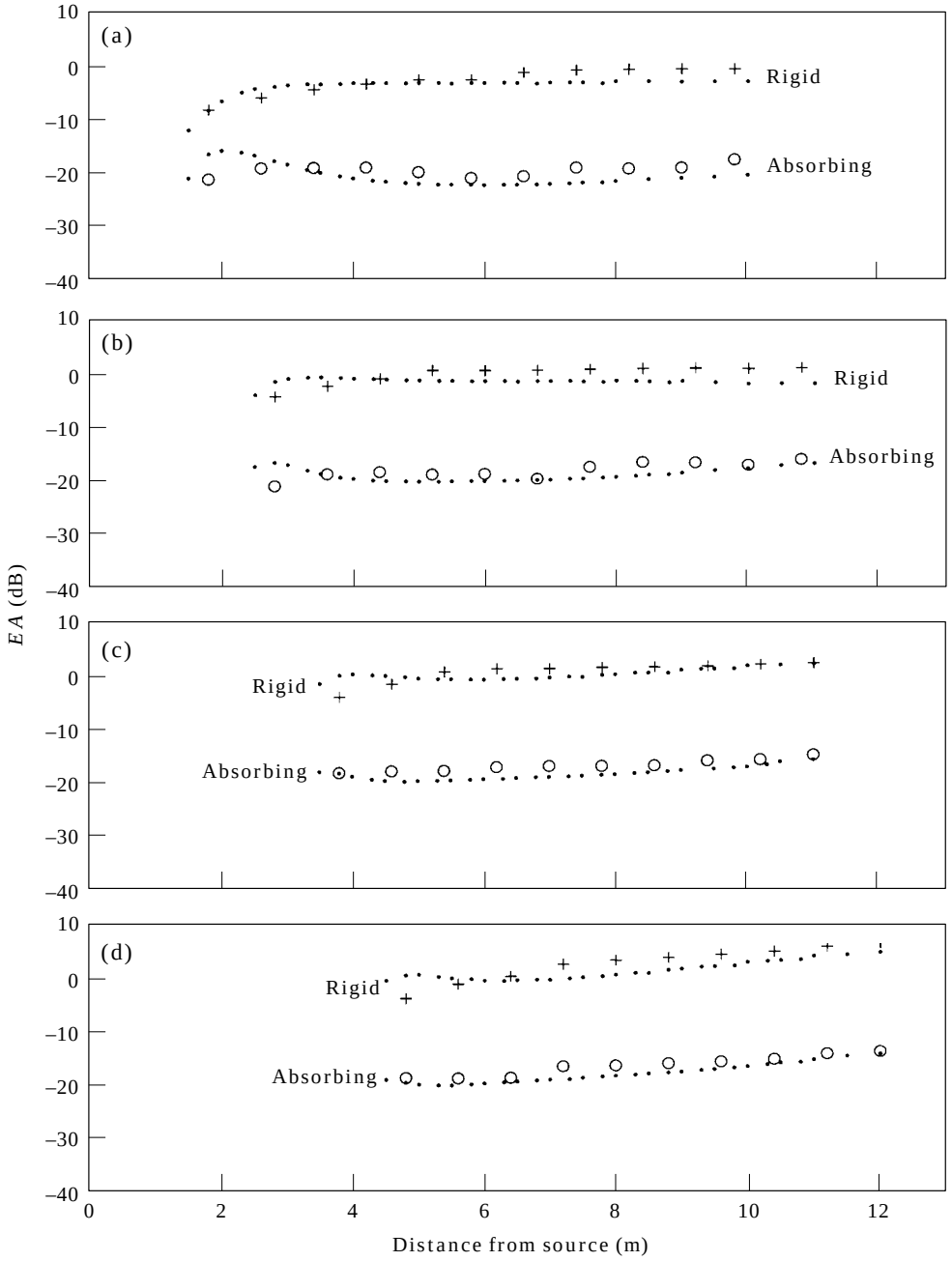

Figure 9. Excess attenuation obtained for a frequency of 500 Hz over concave surfaces in the presence of a barrier. Points: the boundary element method calculations; circles and pulses: experimental measurements. $h_s = 0{\cdot}16$ m, $h_r = 0{\cdot}05$ m, $h_b = 0{\cdot}80$ m, x_{sb} = (a) 1·0 m, (b) 2·0 m, (c) 3·0 m, and (d) 4·0 m.

Next, experimental results and BEM predictions are presented for the case of a convex surface in the presence of a barrier. The plot of *EA* versus the distance along the curved surface from the source is shown in Figure 8. The corresponding results above the rigid and absorbing convex surfaces are presented for the source frequency of 500 Hz. Finally, Figure 9 shows typical results for the case of the sound field above the concave surfaces with the source frequency of 500 Hz. Again, there are good agreements between measurements and BEM predictions for both convex and concave surfaces.

5. INSERTION LOSS OF NOISE BARRIERS IN THE REFRACTING ATMOSPHERE

To study the acoustic performance of a noise barrier in the refracting atmosphere, the total insertion loss (IL_{total}) is frequently used. It is defined as the difference between the sound pressure level in a homogeneous medium and that of the sound pressure level in the refracting atmosphere. With the acoustic analogy, IL_{total} for curved surfaces is defined as the difference between the sound pressure level without a barrier on a flat surface and that of the sound pressure level with a barrier on a curved surface. The total insertion loss of the barrier can be obtained directly from Figures 7–9 and the initial measurements of *EA* without the barrier over the flat surface. Figures 10(a) and (b) show the result of the total insertion loss on the rigid and absorbing surfaces, respectively. In these two figures, the results for flat, concave and convex surfaces are superimposed for ease of comparison.

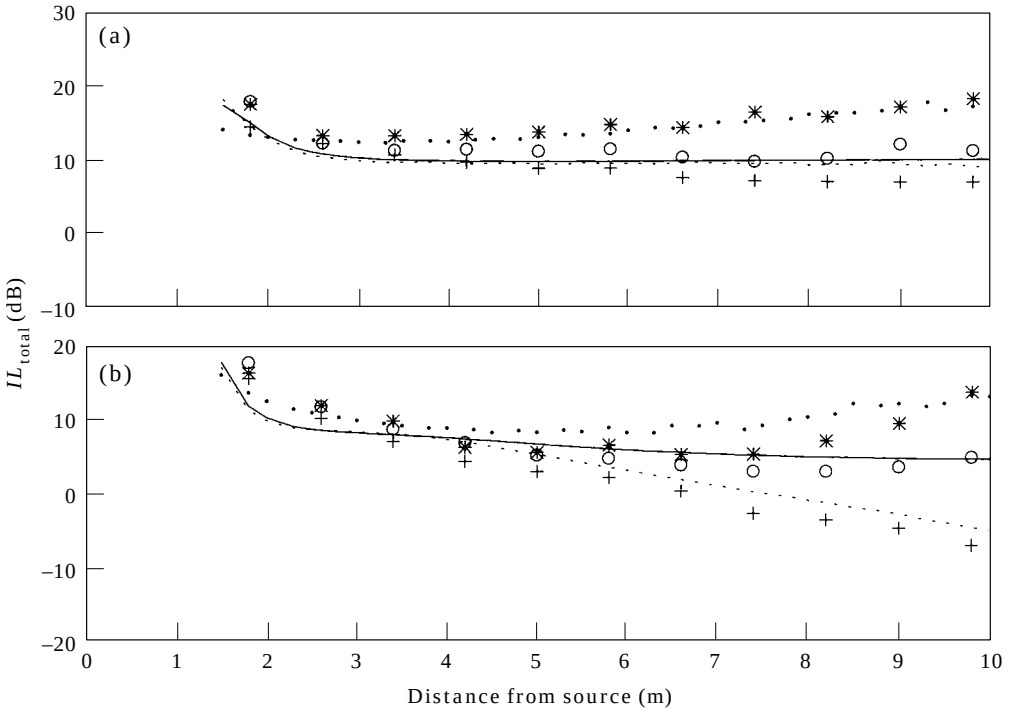

Figure 10. Barrier insertion loss, IL_{total}, obtained for an equivalent full-scale frequency of 500 Hz over (a) rigid surfaces, and (b) absorbing surfaces. Points and stars: the BEM calculations and measurements over convex surfaces; solid lines and circles: the BEM calculations and measurements over flat surfaces; dotted lines and crosses: the BEM calculations and measurements over concave surfaces. $h_s = 0{\cdot}16$ m, $h_r = 0{\cdot}05$ m, $h_b = 0{\cdot}80$ m, $x_{sb} = 1{\cdot}0$ m.

In these typical cases, the barrier is inserted at the scaled distance of 1·0 m from the source and other scaled distances (2·0, 3·0 and 4·0 m) are not shown for brevity. The scale frequency of 500 Hz is used in these two examples. In general, the agreement between the BEM predictions and the measurements is tolerably good for all cases. The experimental and numerical results indicate that the total insertion loss of the barrier is enhanced in the convex surface whilst it is degraded in the concave surface. Consequently, these experimental results support the view that the total insertion loss of barriers is increased for an upward refracting atmosphere and decreased for a downward refracting atmosphere [27].

On the basis of the success reported above, one can extrapolate the BEM result to predict the effectiveness of a noise barrier in a more realistic outdoor environment. The total insertion loss, IL_{total} may not be a good indicator for the acoustic performance of a barrier in a refracting atmosphere. This is because the meteorological effects have been included in the factor, IL_{total}. To assess the effectiveness of a barrier, one can use the barrier insertion loss, IL_{barrier} instead. It is defined as the difference between the sound field above an impedance ground without a barrier and that of the sound field with a barrier. The parameter, IL_{barrier} is related to IL_{total} by

$$IL_{\text{total}} = IL_{\text{barrier}} + IL_{\text{geom}}, \tag{12}$$

where IL_{geom} is the insertion loss due to the effect of refraction. The quantity, IL_{geom}, is defined as the difference between the sound field above an impedance ground in a

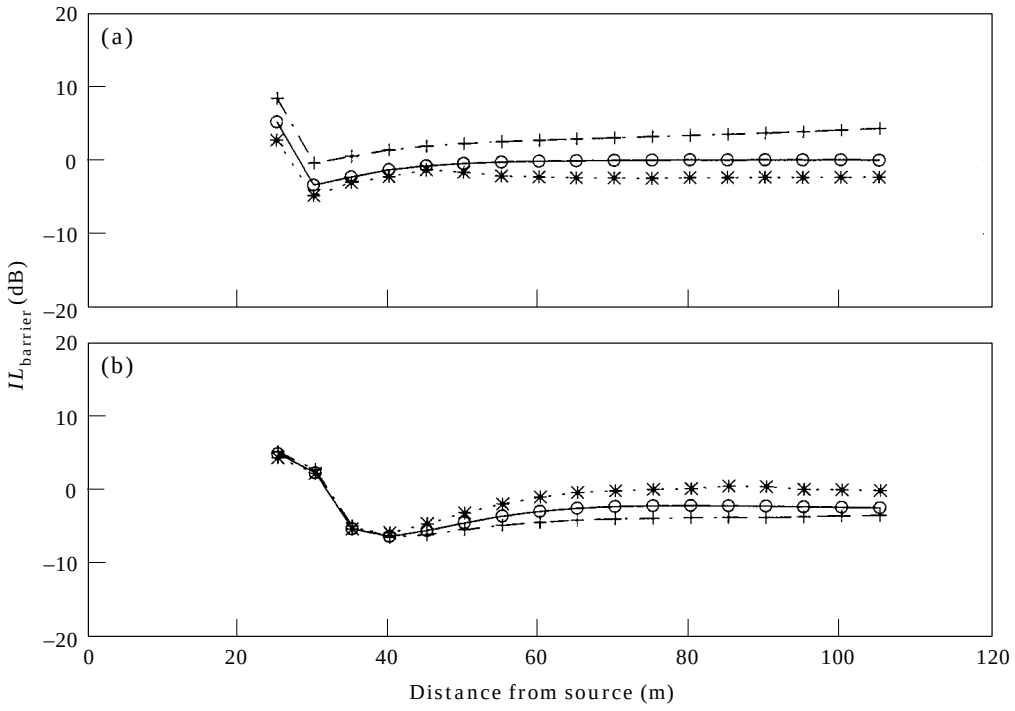

Figure 11. Insertion loss of a barrier, IL_{barrier}, calculated for a frequency of 500 Hz with $h_s = h_r = 2$ m, $x_{sb} = 20$ m and $h_b = 2{\cdot}5$ m. Dotted lines and stars: upward refraction; dashdot lines and pluses: downward refraction; solid lines and circles: no refraction. (a) $\sigma_e = 20$ kPa s^{-1} m^{-2}, $\alpha_e = 60$ m^{-1} and sound speed gradient of $\mp 1{\cdot}0$ s^{-1}; (b) $\sigma_e = 100$ kPa s^{-1} m^{-2}, $\alpha_e = 100$ m^{-1} and sound speed gradient of $\mp 0{\cdot}1$ s^{-1}.

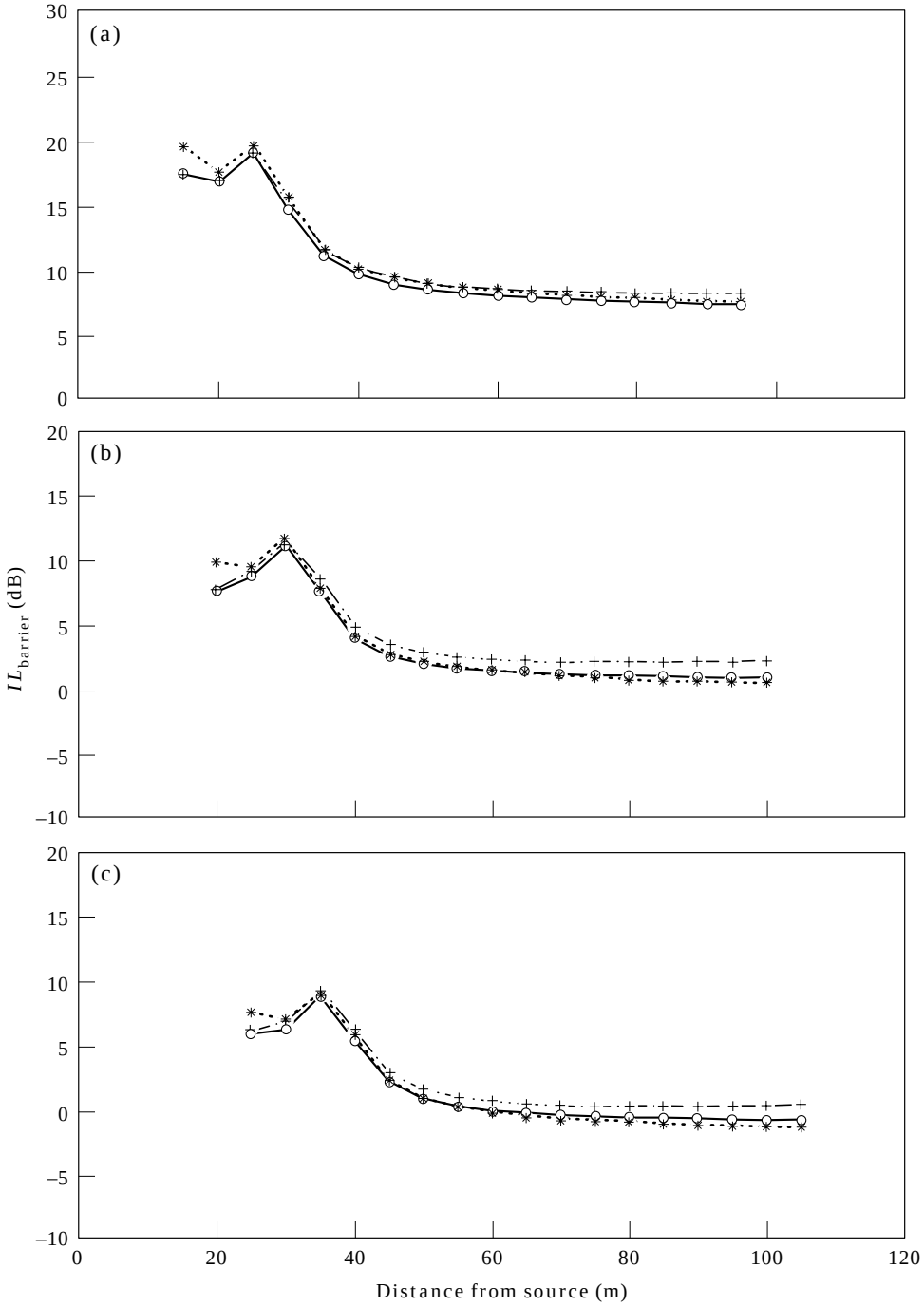

Figure 12. Insertion loss of a barrier, IL_{barrier} calculated for a source frequency of 1 kHz with $\sigma_e = 100$ kPa s^{-1} m^{-2}, $\alpha_e = 100$ m^{-1} and sound speed gradient of ∓ 0.1 s^{-1}. $h_s = 1{\cdot}0$ m, $h_r = 1{\cdot}5$ m and $h_b = 2{\cdot}5$ m. Dotted lines and stars: upward refraction; dashdot lines and pluses: downward refraction; solid lines and circles: no refraction. (a) $x_{sb} = 10$ m, (b) $x_{sb} = 15$ m, and (c) $x_{sb} = 20$ m.

homogeneous medium and that of the sound field in the refracting atmosphere. A typical case is considered in the following numerical examples, where both the source and receiver are situated at 2 m above the impedance ground. The barrier has a height of 2·5 m and is located at a distance of 20 m from a source. Two types of impedance ground with $\sigma_e = 20$ kPa s^{-1} m^{-2}, $\alpha_e = 60$ m^{-1} and $\sigma_e = 100$ kPa s^{-1} m^{-2}, $\alpha_e = 100$ m^{-1}, respectively, are used to simulate the conditions of a soft and a hard ground. Figures 11(a) and (b) show the calculated barrier insertion loss as a function of range for a source frequency of 500 Hz. The results are presented for an upward refracting medium (stars and dotted lines), a downward refracting medium (crosses and dashdot lines), and a homogeneous medium (circles and solid lines). The effective sound speed gradients $\mp 1{\cdot}0$ s^{-1} and $\mp 0{\cdot}1$ s^{-1} were used in the numerical calculations for Figures 11(a) and (b), respectively.

Similar to Figure 11(b), Figures 12 and 13 show the predicted barrier insertion losses for different source frequencies and various ranges. In Figure 12, the barrier insertion loss is plotted as a function of range for a frequency of 1 kHz with source and receiver heights of 1·0 and 1·5 m, respectively. The barrier is located at various distances of 10, 15 and 20 m from the source respectively. Figure 13 shows the predicted barrier insertion loss as a function of source frequency for different sources–barrier–receiver geometries. Figure 13(a) shows the results calculated for the receiver height of 1·5 m that is located at a horizontal distance of 50 m from the barrier. On the other hand, Figure 13(b) shows the results calculated for a receiver located at 2·0 m above the ground and at a horizontal distance of 80 m from the barrier. The barrier source heights are the same as those used in

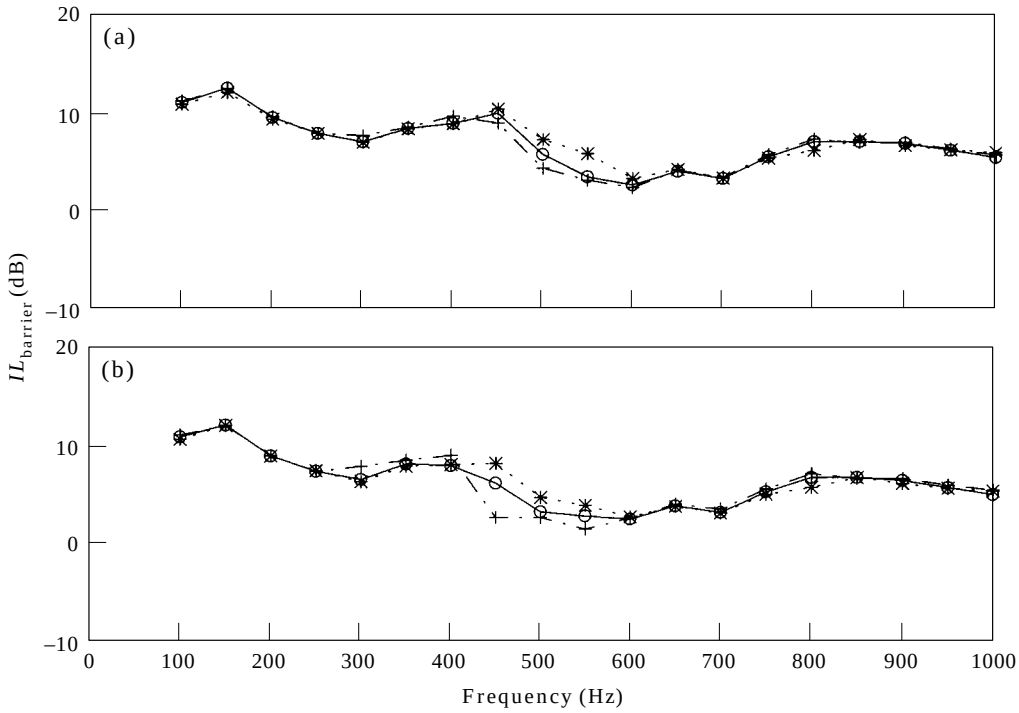

Figure 13. Insertion loss of a barrier, IL_{barrier}, calculated with $\sigma_e = 100$ kPa s^{-1} m^{-2}, $\alpha_e = 100$ m^{-1} and sound speed gradient of $\mp 0{\cdot}1$ s^{-1}. $h_s = 2$ m, $x_{sb} = 10$ m and $h_b = 2{\cdot}5$ m. Dotted lines and stars: upward refraction; dashdot lines and pluses: downward refraction; solid lines and circles: no refraction. (a) $h_r = 1{\cdot}5$ m and $x_{bm} = 50$ m; (b) $h_r = 2{\cdot}0$ m and $x_{bm} = 80$ m.

Figure 11. In both cases, the distance between the source and the barrier is 10 m, the impedance ground is calculated with $\sigma_e = 100$ kPa s^{-1} m^{-2}, $\alpha_e = 100$ m^{-1} and the effective sound speed gradients are $\mp 0{\cdot}1$ s^{-1}.

Note, from Figures 11–13, that the insertion loss is dependent on the source/receiver geometry, source frequency, effective sound speed gradient, barrier height and ground impedance. To confirm the trend, other source/receiver configurations have also been tried and the distance of the source from the barrier varied in the other numerical calculations (results not shown). It was found that the barrier insertion loss in the refracting atmosphere is significantly different from that of the homogeneous atmosphere. There is no consistent trend to support the view that the barrier insertion loss is always higher in the case of a downward or upward refracting medium. Consequently, these numerical "experiments" suggest that the effectiveness of a noise barrier is *not* necessarily degraded in a downward refracting atmosphere and is *not* obviously enhanced in an upward refraction atmosphere. The meteorological influence on sound propagation plays a significant role in determining the effectiveness of a noise barrier.

6. CONCLUSIONS

A rigorous numerical approach, based on a conformal transformation and the boundary element method (BEM), has been used to compute the sound field behind noise barriers in a refracting atmosphere. The numerical results have been validated by a series of scale model experiments in which the curved surfaces are used to simulate sound propagation in the refracting atmosphere. Also results of the current numerical scheme have been compared with published experimental results. In general, there is a good agreement between the BEM predictions and the experimental measurements for all cases.

In this paper, a novel approach involving the use of curved surfaces has been proposed to assess the acoustic performance of noise barriers. It is possible, by combining the BEM and conformal transformation, to examine the effects of sound speed gradient on barrier insertion loss. The experimental measurements and numerical calculations confirm the general belief that the total insertion loss of a barrier is degraded in a downward refracting medium and enhanced in an upward refracting medium. However, this apparent change in the acoustic performance of a noise barrier is largely due to the meteorological influence on sound propagation outdoors. Finally, the effectiveness of a noise barrier in a refracting atmosphere was studied by considering the barrier insertion loss. The numerical results suggest that the effectiveness of a barrier depends on a number of factors such as the source/receiver geometry, the effective sound speed gradient, the source frequency, the barrier height and the impedance of the ground surface.

ACKNOWLEDGMENTS

The work reported in this paper was supported in part by EPSRC through grant reference GR/L 15236. We gratefully acknowledge the Research Committee of the Open University for financial support. Q.W. was supported by an Open University Competitive Studentship. We wish to thank Professor Keith Attenborough for illuminating discussions and to Dr Simon Chandler-Wilde for providing us with a copy of his BEM program.

REFERENCES

1. W. E. Scholes, A. C. Salvidge and J. W. Sargent 1970 *Journal of Sound and Vibration* **16**, 627–642. Field performance of a noise barrier.

2. W. E. Scholes and J. W. Sargent 1971 *Applied Acoustics* **4**, 203–234. Performance of a motorway noise barrier at Heston.
3. W. E. Scholes, A. M. Mackie, G. H. Vulkan and D. G. Harland 1974 *Applied Acoustics* **7**, 1–13. Performance of a motorway noise barrier at Heston.
4. Z. Maekawa 1965 *Applied Acoustics* **1**, 157–173. Noise reduction by screens. See also *Mem. Faculty of Engineering Kobe University* **11**, 29–53 (1965).
5. G. Reinhold 1971 *Strassenbau und Strassenverkehrstechnik* **119**, Bundesminister für Verkehr, Bonn, Germany. Bau- und und verkehrstechnische Massnahmen zum Schutz gegen Verkehrslarm (Designing for the control of road traffic).
6. R. H. Bolt and E. A. G. Shaw 1971 *Journal of the Acoustical Society of America* **50**, 443–445. Initial program of the Co-ordinating Committee on Environmental Acoustics.
7. U. J. Kurze 1974 *Journal of the Acoustical Society of America* **55**, 504–518. Noise reduction by barriers.
8. J. R. Johnston 1995 *Proceedings of Institute of Acoustics* **17**, 109–113. Environmental noise barriers—M25 widening Junctions 10–11.
9. G. R. Watts, D. H. Crombie and D. C. Hothersall 1994 *Journal of Sound ad Vibration* **177**, 289–305. Acoustic performance of new designs of traffic noise barriers—full scale tests.
10. D. S. Jones 1972 *Journal of Sound and Vibration* **20**, 71–78. Diffraction theory: a brief introduction review.
11. A. D. Pierce 1974 *Journal of the Acoustical Society of America* **55**, 941–955. Diffraction of sound around corners and over wide barriers.
12. T. Isei, T. F. W. Embleton and J. F. Piercy 1980 *Journal of the Acoustical Society of America* **67**, 46–58. Noise reduction by barriers on finite impedance.
13. A. L'Esperance, J. Nicolas and G. A. Daigle 1989 *Journal of the Acoustical Society of America* **86**, 1060–1064. Insertion loss of absorbent barriers on ground.
14. A. L'Esperance 1989 *Journal of the Acoustical Society of America* **86**, 179–183. The insertion loss of finite length barriers on the ground.
15. Y. L. Lam and S. C. Roberts 1993 *Journal of the Acoustical Society of America* **93**, 1445–1455. A simple method for accurate prediction of finite barrier insertion loss.
16. D. C. Hothersall, S. N. Chandler-Wilde and M. N. Hajmirzae 1991 *Journal of Sound and Vibration* **146**, 303–322. Efficiency of single noise barriers.
17. E. M. Salomons 1996 *Applied Acoustics* **47**, 217–238. Noise barriers in a refracting atmosphere.
18. S. N. Chandler and D. C. Hothersall 1985 *Journal of Sound and Vibration* **98**, 475–491. Sound propagation above an inhomogeneous impedance plane.
19. Y. L. Li, S. J. Franke and C. H. Liu 1993 *Journal of the Acoustical Society of America* **94**, 1067–1075. Wave scattering from a ground with a Gaussian bump or trough in an inhomogeneous medium.
20. K. M. Li, Q. Wang and K. Attenborough 1997 *Journal of the Acoustical Society of America* (submitted). Analytical approximations for the 3-D sound fields due to a monopole and dipole sources over convex surfaces.
21. P. M. Morse and H. Feshbach 1953 *Methods of Theoretical Physics*, Part I. New York: McGraw Hill Book Company. See pp. 499–508.
22. K. Attenborough, S. Taherzadeh, H. E. Bass, X. Di, R. Raspet, G. R. Becker, A. Güdesen, A. Chrestman, G. A. Daigle, A. L'Espérance, Y. Gabillet, K. Gilbert, Y. L. Li, M. J. White, P. Naz, J. M. Noble and H. A. J. M. van Hoof 1995 *Journal of the Acoustical Society of America* **97**, 173–191. Benchmark cases for outdoor sound propagation models.
23. K. Attenborough 1992 *Journal of the Acoustical Society of America* **92**, 418–427. Ground parameter information for propagation modelling.
24. K. Attenborough, K. M. Li and S. Taherzadeh 1995 *Proceedings of InterNoise* 95 **1**, 319–322. Propagation from a broad-band source over grassland: comparison of data and model.
25. Y. Gabillet, H. Schroeder, G. A. Daigle and A. L'Esperance 1993 *Journal of the Acoustical Society of America* **93**, 3105–3116. Application of the Gaussian beam approach to sound propagation in the atmosphere: theory and experiments.
26. K. B. Rasmussen 1996 *Journal of the Acoustical Society of America* **100**, 3581–3586. Sound propagation over screened ground under upwind conditions.
27. R. De Jong and E. Stusnick 1976 *Noise Control Engineering* **6**, 101–109. Scale model studies of the effects of wind on acoustic barrier performance.
28. Q. Wang 1997 *Ph.D. Thesis*, *The Open University*. Atmospheric refraction and propagation over curved surfaces.